The Formulation and Atmospheric Simulation of the Community Atmosphere Model Version 3 (CAM3)

WILLIAM D. COLLINS, PHILIP J. RASCH, BYRON A. BOVILLE, JAMES J. HACK, JAMES R. MCCAA, DAVID L. WILLIAMSON, AND BRUCE P. BRIEGLEB

National Center for Atmospheric Research, Boulder, Colorado

CECILIA M. BITZ

Atmospheric Sciences, University of Washington, Seattle, Washington

SHIAN-JIANN LIN

Geophysical Fluid Dynamics Laboratory, Princeton, New Jersey

MINGHUA ZHANG

State University of New York at Stony Brook, Stony Brook, New York

(Manuscript received 31 January 2005, in final form 1 September 2005)

ABSTRACT

A new version of the Community Atmosphere Model (CAM) has been developed and released to the climate community. CAM Version 3 (CAM3) is an atmospheric general circulation model that includes the Community Land Model (CLM3), an optional slab ocean model, and a thermodynamic sea ice model. The dynamics and physics in CAM3 have been changed substantially compared to implementations in previous versions. CAM3 includes options for Eulerian spectral, semi-Lagrangian, and finite-volume formulations of the dynamical equations. It supports coupled simulations using either finite-volume or Eulerian dynamics through an explicit set of adjustable parameters governing the model time step, cloud parameterizations, and condensation processes. The model includes major modifications to the parameterizations of moist processes, radiation processes, and aerosols. These changes have improved several aspects of the simulated climate, including more realistic tropical tropopause temperatures, boreal winter land surface temperatures, surface insolation, and clear-sky surface radiation in polar regions. The variation of cloud radiative forcing during ENSO events exhibits much better agreement with satellite observations. Despite these improvements, several systematic biases reduce the fidelity of the simulations. These biases include underestimation of tropical variability, errors in tropical oceanic surface fluxes, underestimation of implied ocean heat transport in the Southern Hemisphere, excessive surface stress in the storm tracks, and offsets in the 500-mb height field and the Aleutian low.

1. Introduction

The Community Atmosphere Model (CAM3) represents the sixth generation of atmospheric general circulation models (AGCMs) developed by the climate community in collaboration with the National Center for Atmospheric Research (NCAR). Like its predecessors, CAM is designed to be a modular and versatile model suitable for climate studies by the general scientific community (Collins et al. 2004). CAM3 can be run either as a stand-alone AGCM or as a component of the Community Climate System Model (CCSM; Collins et al. 2006a). In its stand-alone mode, CAM3 is integrated together with the Community Land Model (CLM; Bonan et al. 2002; Oleson et al. 2004), a thermodynamic sea ice model, and a data ocean or optional slab ocean model. In its coupled mode, CAM3 is integrated together with the CLM, the Community Sea Ice Model (CSIM5; Briegleb et al. 2004), and the Parallel Ocean Program (POP; Smith and Gent 2002). The thermody-

Corresponding author address: Dr. William D. Collins, NCAR, P.O. Box 3000, Boulder, CO 80307.
E-mail: wcollins@ucar.edu

namic sea ice model for the stand-alone mode is derived from CSIM5. The stand-alone mode is particularly suitable for examining the response of the atmospheric circulation and state to observed patterns and changes in sea surface temperature. It can also be used to estimate the equilibrium response to external forcings, for example anthropogenic increases in atmospheric carbon dioxide. The coupled model is suitable for studying the interactions of the atmosphere, ocean, sea ice, and land surface on seasonal to millennial time scales.

The first four versions of the atmospheric model were in a series of Community Climate Models (CCM) starting with CCM0 (Washington 1982; Williamson 1983), continuing with CCM1 (Williamson et al. 1987) and CCM2 (Hack et al. 1993), and ending with CCM3 (Kiehl et al. 1998). CCM3 was the first version with the flexibility to run either as a stand-alone AGCM or as a component of the coupled Climate System Model (CSM1; Boville and Gent 1998). This extension to the functionality prompted several changes in the nomenclature of the models. After the release of CCM3 and CSM1, the developers decided to rename the AGCM as the Community Atmosphere Model (CAM) and the coupled framework as the CCSM. CAM2 and CCSM2 were released to the climate community in May 2002 (Kiehl and Gent 2004). It soon became evident that CAM2 and CCSM2 exhibited a number of systematic biases that needed to be addressed to improve the fidelity of the climate simulations. These include high boreal winter land surface temperatures, low tropical tropopause temperatures, biases in surface fluxes in coastal stratus regions, relatively weak tropical variability, and errors in the structure of the intertropical convergence zones (ITCZs). After another cycle of analysis and development, CCSM3 and CAM3 were released to the climate community in June 2004. The code, documentation, input datasets, and model simulations for CAM3 are freely available from the CAM Web site (http://www.ccsm.ucar.edu/models/atm-cam). As we will show, the development effort succeeded in reducing several of these biases in CAM2 and CCSM2. The comparisons are based upon stand-alone integrations of CAM using Eulerian spectral dynamics with T85 spectral truncation for CAM3 and T42 truncation for earlier versions. The implementation of CAM3 with T85 spectral dynamics is the version used in CCSM3 simulations for international assessments of climate change.

This paper will discuss the new physics and dynamics in CAM3, summarize basic aspects of the climate simulation, and describe and analyze some of the improvements in the climate simulation relative to previous, versions. The properties include the global energetics, thermodynamic profiles, global and zonal-mean characteristics of the hydrological cycle, and meridional transports of heat and moisture. The mean state and transient behavior of the simulated hydrological cycle are discussed in Hack et al. (2006) and Rasch et al. (2006b), and the dynamic circulation is described in Hurrell et al. (2006). Other aspects of the atmospheric simulation and improvements in the simulation fidelity are discussed in the overview of CCSM3 by Collins et al. (2006a). It is important to note that some of the changes in the climate simulation are related to the modifications to the land surface model. The changes related to improvements in CLM are discussed by Bonan et al. (2002).

The new formulations of physics and dynamics are outlined in section 2. A more complete technical description of the physical basis and numerical implementation of these changes is given in Collins et al. (2004). The mean features of the atmospheric state, energetics, and energy transport are presented in section 3. The reduction in model biases relative to previous versions is discussed in section 4. Several of the main biases remaining in the climate simulation from CAM3 are described in section 5, followed by a summary in section 6.

2. Overview of new physics and dynamics

a. Dynamical frameworks

Previous versions of CAM have included Eulerian spectral and semi-Lagrangian dynamics. CAM3 includes the finite volume (FV) dynamical core (Lin and Rood 1996; Lin 2004), and its initial applications include simulations of atmospheric chemical transport and chemical processes (Boville and Rasch 2005, unpublished manuscript; Rasch et al. 2006a). The physical parameterizations have been completely separated from the dynamical core, and the dynamics can be coupled to the physics in a time-split or process-split approximation (Williamson 2002). In the process-split technique, the calculations of dynamical and physical tendencies for prognostic variables are based upon the same past state. In the time-split technique, the tendencies for dynamics and physics are computed sequentially, each based upon the state produced by the other. In CAM3, the physics and Eulerian or semi-Lagrangian dynamical cores are process split, while the physics and FV core are time split for reasons discussed in Williamson (2002). Within the physical parameterization package, individual parameterizations are time split.

CAM3 has been designed to produce simulations with reasonable fidelity for several different dynamical cores and horizontal resolutions. In the absence of any modifications to the physical parameterizations, changes

in resolution and dynamics both introduce perturbations in the mean climate and the top-of-model (TOM) energy balance of CAM3. To run CAM3 as part of a stable coupled system, the energy balance in each configuration is established by adjusting twelve parameters governing the cloud condensate, cloud amount, precipitation processes, and biharmonic diffusion (Collins et al. 2004). The model time step is also adjusted to satisfy the Courant–Friedrichs–Levy (CFL) condition when Eulerian dynamics is used. In its current implementation, the adjustable parameters have been configured for the Eulerian dynamical core at T31, T42, and T85 spectral truncations and for the FV core at $2° \times 2.5°$ horizontal resolution. The Eulerian truncations correspond to zonal resolutions ranging from 3.87° for the T31 configuration to 1.41° for the T85 configuration.

b. New treatment of cloud and precipitation processes

The treatments of microphysics and cloud condensate have been substantially revised in CAM3 (Boville et al. 2006). The diagnostic cloud water scheme used in CCM3 has been replaced by the prognostic cloud water parameterization of Rasch and Kristjánsson (1998) updated by Zhang et al. (2003). The new model includes separate evolution equations for the liquid and ice-phase condensate. The revised scheme includes a new formulation of the fractional condensation rate and a self-consistent treatment of the evolution of water vapor, heat, cloud fraction, and in-cloud condensate (Zhang et al. 2003). The net effect of these changes is to double the global amount of cloud condensate, with the largest increases occurring in the storm tracks (Fig. 1; Hack et al. 2006). Condensed water detrained from shallow and frontal convection can either form precipitation or additional stratiform cloud water. Convective precipitation can evaporate into its environment at a rate determined from Sundqvist (1988). The latent heats of vaporization and fusion are applied consistently to transformations involving liquid and ice-phase condensate and precipitation, respectively.

Advection and sedimentation of cloud droplets and ice particles are included in the equations governing cloud condensate. The settling velocities for liquid and ice-phase constituents are computed separately as functions of particle size characterized by the effective radius. Small ice particles are assumed to fall like spheres according to the Stokes equation. As the size of the ice particles increases, there is a smooth transition to a different formula for fall speeds following Locatelli and Hobbs (1974). The fall velocities of liquid drops are treated using the Stokes equation for their entire size range.

In CAM3, cloud fraction is derived from diagnostic relationships for the amounts of low-level marine stratus, shallow and deep convection, and layered cloud systems. The parameterization for marine stratus is similar to that used in CAM2. It is based upon the empirical relationship between atmospheric stratification and stratocumulus cloud fraction obtained by Klein and Hartmann (1993). The treatment of cirrus anvil area used in CAM2 has been replaced with expressions for shallow and deep convective cloud fractions as functions of convective updraft mass flux following Xu and Krueger (1991). The layered cloud fraction is diagnosed from relative humidity. The quadratic expression contains a set of parameters for the minimum humidity required to form clouds in the lower and upper atmosphere that are adjusted depending on the horizontal resolution of the model.

c. Radiative processes

The radiative parameterizations have been updated to include new treatments of the interactions of shortwave and longwave radiation with cloud geometry and with water vapor. The modifications to cloud overlap and longwave interactions were originally introduced in CAM2, and the shortwave absorption by water vapor has been modified in CAM3. The new, generalized formulation for cloud geometry can calculate the radiative fluxes and heating rates for any arbitrary combination of maximum and random cloud overlap (Collins 2001b). The type of overlap is completely separated from the radiative parameterizations, and it can vary from one grid cell or time step to the next. In practice, CAM3 applies a standard maximum-random cloud overlap scheme (Zdunkowski et al. 1982) to all cloud configurations. The parameterizations are mathematically equivalent to the independent column approximation (ICA) and reproduce ICA solutions to within user-selectable limits.

The absorption and emission of longwave radiation by water vapor have been updated using modern spectral line databases and recent approximations for the water vapor continuum. The parameterizations for these terms used in CCM3 have been replaced with new parameterizations developed using the Hitran2K line data and its 2001 update (Rothman et al. 2003) together with the Clough–Kneizys–Davies (CKD) 2.4.1 model for the continuum based upon Clough et al. (1989). The terms are derived from line-by-line radiative calculations using the methodology of Collins et al. (2002a). These changes increase the cooling at 300 mb due to line absorption and the foreign continuum in the rotation band, and they decrease the cooling near 800 mb due to the self-continuum in the rotation band. The

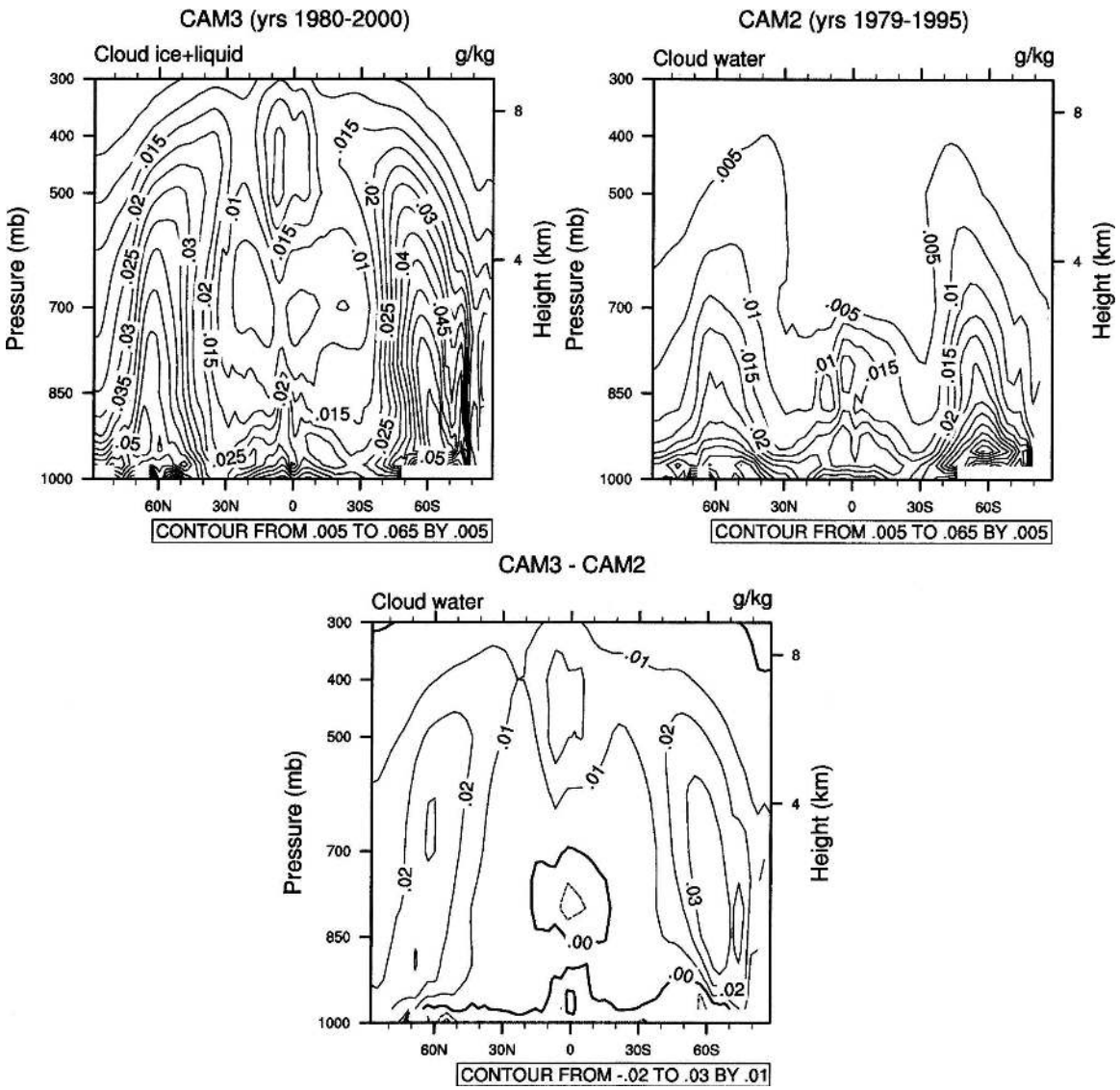

FIG. 1. Vertical profiles of the mixing ratio of cloud condensate (annually and zonally averaged) in CAM3, CAM2, and the difference between CAM3 and CAM2.

changes in the vertical profile of longwave cooling interact with the parameterized convection in a manner consistent with the theory of radiative–convective equilibrium.

The absorption of near-infrared radiation by water vapor has been updated using the same modern line data and approximation for the continuum (Collins et al. 2006b). The global-mean clear-sky and all-sky shortwave absorption increase by 4.0 and 3.1 W m^{-2}, respectively, in calculations replacing the old with the new spectroscopic parameters (Fig. 2). The main changes in the water-vapor spectroscopy responsible for the increased absorption are the addition of many missing weak lines and increased estimates of line strength. The atmosphere becomes warmer, moister, and more stable with the increased absorption.

d. Atmospheric aerosols

In its default configuration, CAM3 includes the radiative effects of an aerosol climatology in the calculation of shortwave fluxes and heating rates. This climatology replaces the globally uniform sulfate aerosol distribution used in previous versions of CCM (Kiehl et al. 1996). The new aerosol dataset includes the annually cyclic, monthly mean distributions of sulfate, sea salt, carbonaceous, and soil–dust aerosols. The climatology is derived from a chemical transport model constrained by assimilation of satellite retrievals of aerosol depth

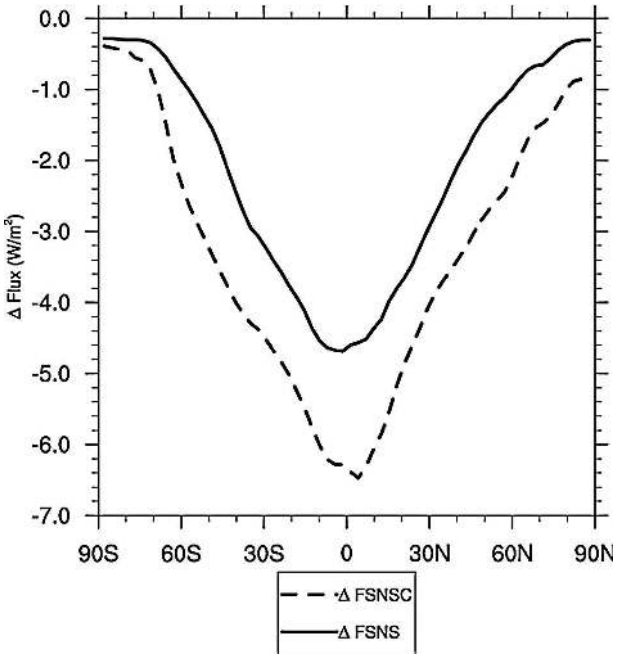

FIG. 2. Change in surface net shortwave flux due to the enhancement in near-infrared absorption by water vapor (annually and zonally averaged) for all-sky conditions (solid, denoted by FSNS) and clear-sky conditions (dashed, denoted by FSNSC).

(Collins et al. 2001; Rasch et al. 2001). The climatology in CAM3 is obtained from an aerosol assimilation for the period 1995–2000. The effects of the aerosols on the shortwave fluxes and heating rates are calculated following Collins et al. (2002b). The radiative effects are particularly significant in regions with large concentrations of natural and anthropogenic aerosols, including the equatorial Atlantic and Indian Oceans, Eastern Europe and Asia, and northern Africa (Fig. 3). In place of the sulfate climatology, the sulfate aerosols can also be predicted using a representation of the sulfur cycle developed by Barth et al. (2000) and Rasch et al. (2000). The effects of volcanic aerosols released by eruptions during the nineteenth and twentieth centuries are obtained from a reconstruction by Ammann et al. (2003).

e. Slab ocean and sea ice models

The sea ice and optional slab ocean models in CAM3 are designed to emulate the surface exchanges in the fully coupled CCSM3 without incurring the computational expense of ocean and ice dynamics. These models are frequently used to estimate the equilibrium response to external forcings, for example increased concentrations of carbon dioxide or anthropogenic aerosols. The vertically integrated heat content in the slab ocean is represented by a single temperature at each grid point. For each ocean grid point and month, a net heat removal rate out of the slab ocean is specified to maintain the climatological observed annual cycle of sea surface temperature (SST). This heat removal rate is computed as the residual from the surface heat budget of an uncoupled simulations forced with observed SSTs and ice cover (Collins et al. 2004). The geographic structure of the monthly mean ocean mixed-layer depth is derived from the vertical profiles of observed ocean salinity (Levitus 1982). The depths in the Tropics range between 10 and 30 m, while at high latitudes the depths vary from 10 m to a specified cap of 200 m.

CAM3 includes a revised thermodynamic sea ice model that uses much of the same physics as the full dynamic sea ice model CSIM5 in CCSM3. The thermodynamic model simulates the snow depth, surface tem-

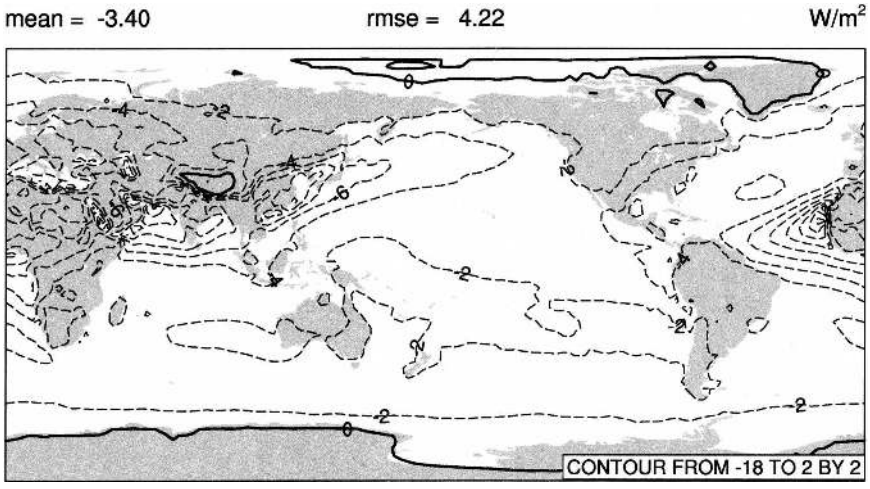

FIG. 3. Difference in the net TOM clear-sky shortwave flux (annually averaged) between calculations with and without the aerosol climatology in CAM3. Dashed contours denote a decrease in TOM flux.

perature, ice thickness, ice fractional coverage, and energy exchange in a four-layer representation of the sea ice. It is designed to operate in two modes depending upon the source of sea surface temperatures. If SSTs are obtained from a boundary dataset, then ice coverage is also input from a dataset. The ice thicknesses are set to 2 m in the Northern Hemisphere and 0.5 m in the Southern Hemisphere. In this case, the sea ice model is just used to compute energy fluxes between the ice and overlying atmosphere. If the SSTs are computed using the slab ocean model, the ice coverage and thickness are calculated by the sea ice model.

f. Heating, kinetic energy dissipation, and vertical diffusion

The calculation of thermodynamic tendencies has been reformulated to insure conservation of energy (Boville and Bretherton 2003). Dry static energy is predicted by each physical parameterization and is updated following each parameterization. The evolution of the temperature and geopotential are then obtained from the updated dry static energy. The dissipation of kinetic energy from vertical diffusion of momentum is calculated explicitly and included in the heating applied to the atmosphere. The parameterization for vertical diffusion has been also generalized to include molecular diffusion above the mesopause and to permit diffusive separation of constituents of different molecular weights. The standard version of CAM3 does not extend to the mesopause and does not include molecular diffusion and viscosity as active processes.

g. Boundary data for orography, sea ice extent, and sea surface temperatures

The datasets used for sea surface temperature, sea ice concentration, and subgrid orographic variations have been replaced with new versions in CAM3. The sea surface temperatures and sea ice concentrations are used in stand-alone integrations of the CAM3. These datasets prescribe analyzed monthly midpoint mean values of SST and ice concentration for the period 1950 through 2001. The datasets are blended products that combine the global Hadley Centre Sea Ice and Sea Surface Temperature (HadISST) dataset (Rayner et al. 2003) for years up to 1981 and the Reynolds et al. (2002) dataset after 1981. These SST and sea ice data are used in the ensemble of T85 integrations analyzed in this paper.

In the parameterization for orographically generated gravity waves, the subgrid-scale variation of orography determines the streamline displacement and the length scale for averaging other parameters in the wave source function taken from McFarlane (1987). In CAM3, the standard deviation of the surface orography within each grid cell is derived from a digital elevation model with a resolution of 30 arc seconds, or approximately 1 km (EROS Data Center 2004), weighted by the land fraction. Other than these changes, the formulation of gravity wave drag is identical to that used in CCM3 (Kiehl et al. 1998).

Earlier versions of the global atmospheric model (the CCM series) included a simple land–ocean–sea ice mask to define the underlying surface of the model. It is well known that fluxes of freshwater, heat, and momentum between the atmosphere and underlying surface are strongly affected by surface type. CAM3 provides a more accurate representation of flux exchanges from coastal boundaries, island regions, and ice edges by including a fractional specification for land, ice, and ocean. The area occupied by these surface types is described as a fractional portion of the atmospheric grid box. Surface fluxes are calculated separately for each surface type, weighted by the appropriate fractional area, and then summed to provide a mean value for a grid box.

3. Basic properties of the simulated climate and general circulation

The analysis of CAM3 is based upon the average of a five-member ensemble integrated at T85 resolution using observed sea surface temperatures (section 2g) from 1950 to 2000. In these runs, the concentrations of greenhouse gases are held constant at 1990 levels, and the concentrations of aerosols are obtained from a present-day climatology (section 2d). The period analyzed here corresponds to the portion of the satellite data record from 1980 through 2000. The CAM2 integration is conduced at T42 resolution using the same observed sea surface temperatures for 1979–95.

The global annual average properties of the simulation are given in Table 1. In the table, the TOM level is the upper interface of CAM3. The top-of-atmosphere (TOA) values are computed for diagnostic comparisons against satellite observations by including the effects of stratospheric ozone above the TOM level. For the all-sky fluxes at TOA, we use the data from the Earth Radiation Budget Experiment (ERBE; Harrison et al. 1990) as modified by Kiehl and Trenberth (1997). The most significant changes in the shortwave energy budget from CAM2 to CAM3 are related to changes in aerosols, extinction by water vapor, cloud amount, and cloud water path. The increase of 5.2 W m^{-2} in clear-sky TOA absorbed shortwave flux is due primarily to the switch from a uniform background aerosol to a

TABLE 1. Global annual-mean climatological properties of CAM2 and CAM3.

Property	CAM2	CAM3	Observation
Annual mean energy budgets (W m^{-2}, + upward)			
TOM	0.26	−0.44	
Surface	0.49	−0.47	
TOA outgoing longwave radiation (W m^{-2}, + upward)			
All sky	235.7	235.6	234[a]
Clear sky	264.9	266.2	264.4[a]
TOA absorbed solar radiation (W m^{-2}, + downward)			
All-sky	237.7	237.1	234[a]
Clear-sky	286.5	291.7	289.3[a]
Longwave cloud forcing (W m^{-2})	29.2	30.7	30.4[a]
Shortwave cloud forcing (W m^{-2})	−48.9	−54.7	−54.2[a]
Cloud fraction (%)			
Total	60.7	56.1	66.7[b]
Low	31.7	40.1	26.4[b]
Medium	19.2	17.3	19.1[b]
High	43	29.3	21.3[b]
Cloud water path (mm)	0.060	0.122	0.112[c]
Precipitable water (mm)	23.8	24.3	24.6[d]
Latent heat flux (W m^{-2})	82.8	83.8	84.9[e]
Sensible heat flux (W m^{-2})	20.2	17.8	15.8[f]
Precipitation (mm day^{-1})	2.86	2.87	2.61[g]
Net surface longwave radiation (W m^{-2}, + upward)			
All sky	64.2	58.0	49.4[h]
Clear sky	92.2	85.8	78.7[h]
Net surface shortwave radiation (W m^{-2}, + downward)			
All sky	167.7	159.1	165.9[h]
Clear sky	220.6	218.6	218.6[h]

[a] ERBE (Harrison et al. 1990; Kiehl and Trenberth 1997).
[b] ISCCP (visible/infrared cloud amount; Rossow and Schiffer 1999).
[c] Moderate Resolution Imaging Spectroradiometer (MODIS; King et al. 2003).
[d] National Aeronautics and Space Administration (NASA) Water Vapor Project (NVAP); Randel et al. 1996).
[e] ECMWF (Kållberg et al. 2004).
[f] NCEP (Kistler et al. 2001).
[g] GPCP (Adler et al. 2003).
[h] ISCCP FD (Zhang et al. 2004).

more detailed climatology with multiple aerosol species. The albedo of the aerosols in the climatology is less than the albedo of the background aerosol. The reduction by 2.0 W m^{-2} in clear-sky surface insolation is caused by the increased atmospheric absorption of shortwave radiation related to the greater extinction by water vapor and to the introduction of absorptive aerosol species. Both CAM3 and CCSM3 underestimate the all-sky surface insolation in polar regions due to excessive surface shortwave cloud radiative effects (Collins et al. 2006a).

The magnitude of shortwave cloud forcing is greater by 5.8 W m^{-2} in CAM3 despite a reduction in total cloud amount from 60.7% in CAM2 to 56.1% in CAM3. One reason for the increased cloud albedo is the shift in the vertical cloud distributions, with 13.7% less high cloud cover and 8.4% more low cloud cover (Fig. 4). In CAM3, the mean optical thickness of low clouds is greater than the mean optical thickness of high clouds. In addition, the global mean cloud water path in CAM3 is approximately 2 times larger than the cloud water path in CAM2. The combination of the larger shortwave cloud forcing and greater absorption by water vapor and aerosols produces an 8.6 W m^{-2} reduction in the global all-sky surface insolation. The reduction is particularly evident in the Northern Hemisphere (Fig. 5). The largest reduction in insolation relative to CAM2 occurs in the Northern Hemisphere Tropics, and this is also the location of the largest negative bias relative to the International Satellite Cloud Climatology Project (ISCCP) flux data (FD) estimates (Zhang et al. 2004). However, this bias is probably an artifact since ISCCP overestimates the all-sky downwelling flux by 21 W m^{-2} relative to surface radiometers at these latitudes (Table 8, Zhang et al. 2004).

The changes to the infrared absorption and emission by water vapor in CAM3 increase the downwelling longwave flux at the surface and decrease the upwelling flux at TOA (Collins et al. 2002a). As a result of these effects and the decrease in surface mean temperature by 0.69 K, the net all-sky and clear-sky surface longwave fluxes decrease by 6.2 and 6.4 W m^{-2}, respectively. The longwave cloud radiative effects at TOA increase by only 1.5 W m^{-2} and the effects at the surface decrease by just 0.2 W m^{-2} despite the large changes in the vertical distribution of cloud and the doubling of the global mean cloud water path.

The global mean statistics of the hydrological cycle are nearly identical between the two models. The precipitable water increases by 2.1%, the latent heat flux by 1.2%, and the precipitation by 0.3% from CAM2 to CAM3. The zonal-mean difference between evaporation and precipitation, which is a measure of the net exchange of water between the surface and the atmosphere, is the same between the models to within an RMS discrepancy of 0.22 mm day^{-1}. The major change between CAM2 and CAM3 is a reduction in the precipitation in the southern branch of the tropical ITCZ. The zonal mean precipitation at 7°S (the location of the maximum southern rainfall) decreases by 0.7 mm day^{-1}, and the precipitation on the equator increases by 0.3 mm day^{-1}. Compared against the GPCP estimates, CAM3 overestimates the precipitation in the Tropics between 25°N to 25°S by 0.7 mm day^{-1}. CAM3 also underestimates the subtropical precipitation between by 0.4 mm day^{-1} in the midlatitude regions between 30°

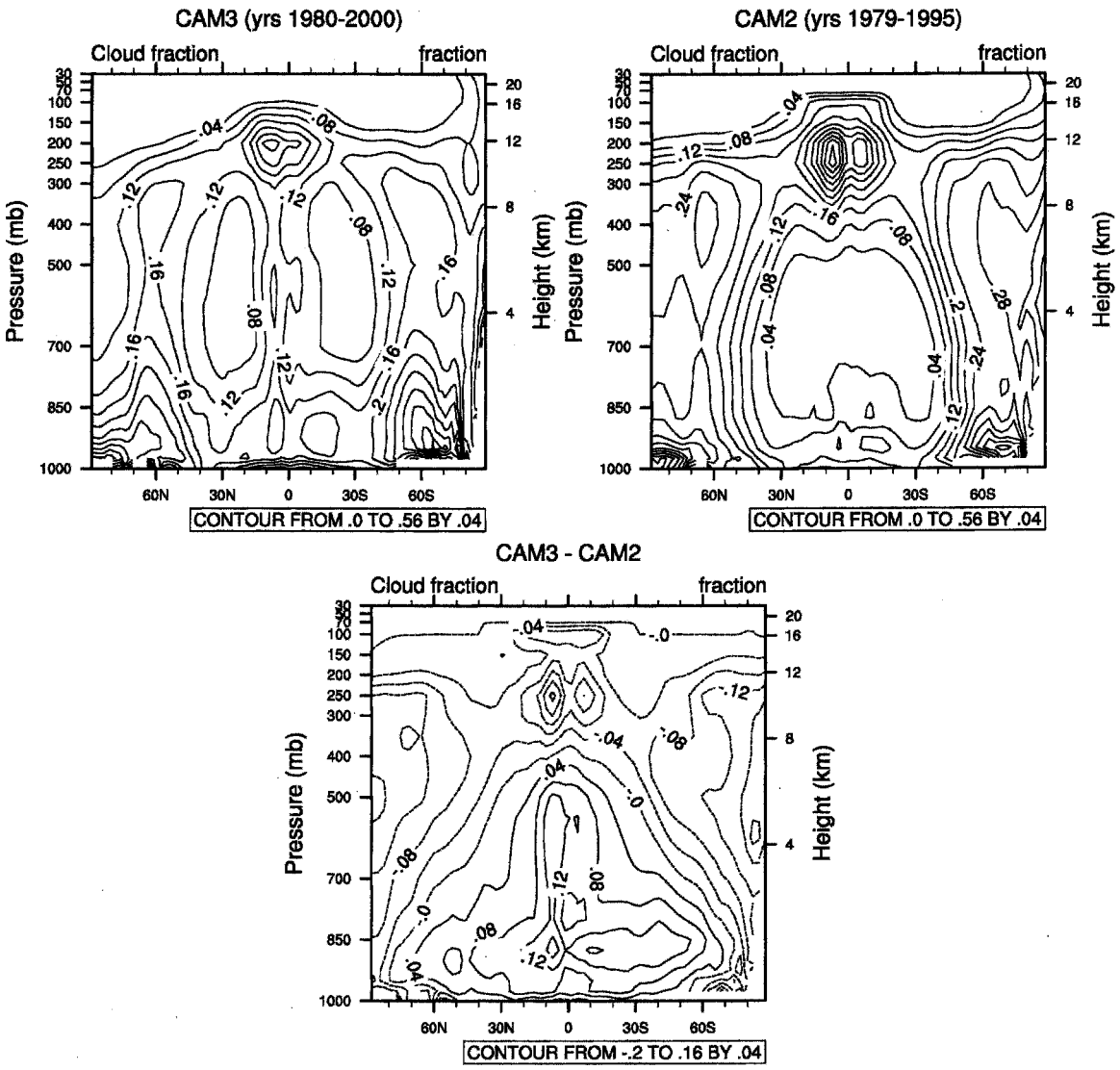

FIG. 4. Vertical profiles of fractional cloud amount (annually and zonally averaged) in CAM3, CAM2, and the difference between CAM3 and CAM2.

to 40°S and 30° to 40°N. Further analysis of the mean hydrological cycle in CAM3 is presented in Hack et al. (2006).

The annual implied northward heat transports for CAM2 and CAM3 are shown in Fig. 6. At each latitude, these transports represent the amount of energy that the ocean, sea ice, and land must transport northward in order to balance the total heat exchanged with the atmosphere between that latitude and the North Pole. In CAM3, the northward heat transport increases by 0.4–0.7 PW between the Tropics and 50°N relative to CAM2. The primary reason is the reduced surface insolation in the new model. Between 5°S and 5°N where the transport increases by 0.69 PW, the effects of the reduced insolation are 2.2 times larger than the changes in other surface fluxes combined. Although the shortwave cloud radiative effects have increased in this region, 71% of the insolation effect is related to the increased absorption by aerosols and water vapor. Like CAM2, CAM3 underestimates the southward transports in the Southern Hemisphere. The maximum error is approximately 1 PW at 10°S.

4. Improvements in the climate simulation and reduction in model biases

The differences in the physics between CAM2 and CAM3 have helped reduce some of the more serious systematic errors in the atmospheric simulations. The focus here is on aspects of the mean climate and its

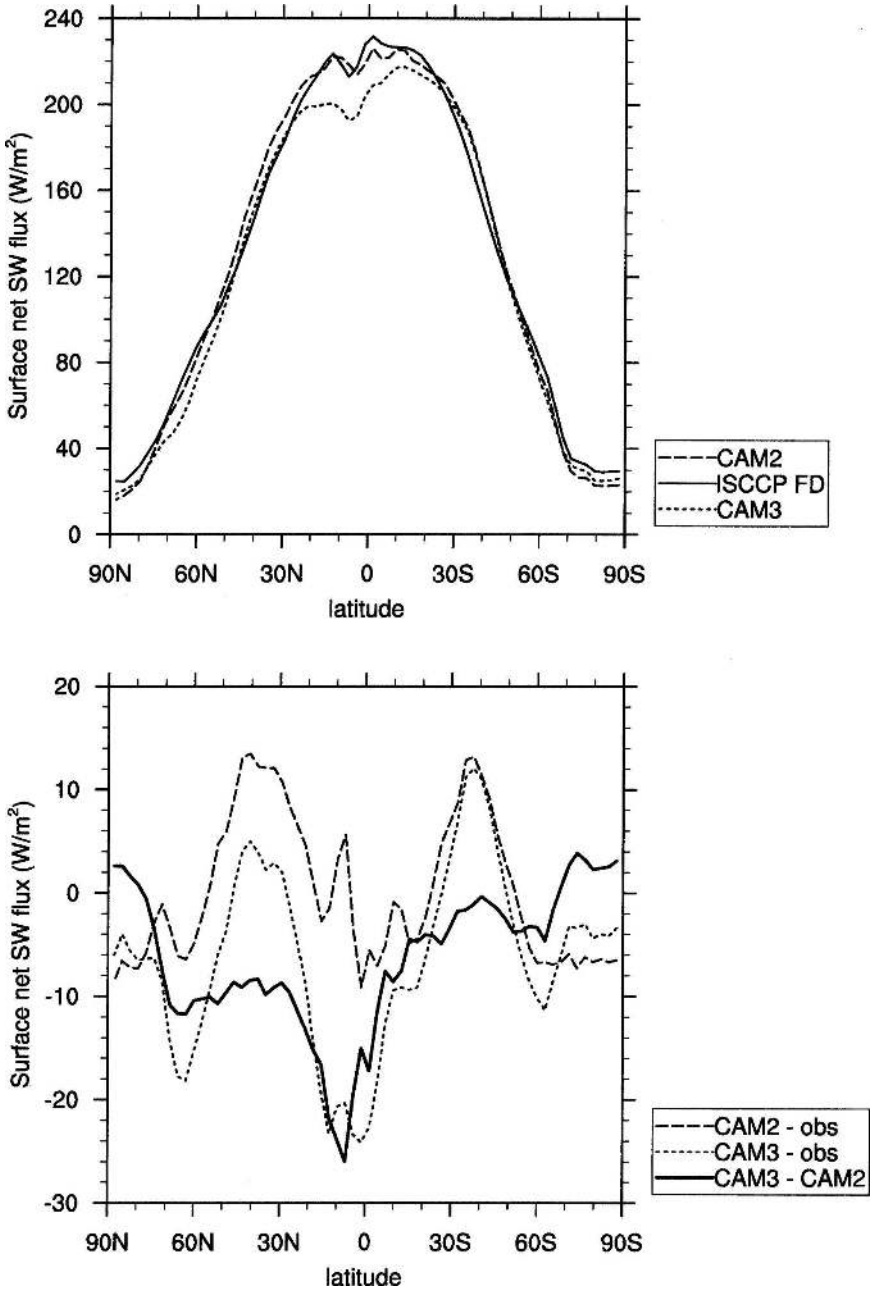

FIG. 5. (top) Net surface shortwave fluxes under all-sky conditions (annually and zonally averaged) from CAM2, CAM3, and the ISCCP FD dataset, and (bottom) differences among the models and ISCCP (obs) estimates.

seasonal variations. The improvements in the boreal winter land surface temperatures, surface insolation, and clear-sky surface radiation in polar regions are discussed in greater detail by Collins et al. (2006a).

a. Temperatures in the upper tropical troposphere

The temperatures for the upper tropical troposphere produced by CAM3 are larger than the temperatures in CAM2 by between 2 and 4 K. A larger cold bias produced by CAM2 near the tropical tropopause has hampered modeling the exchange of water vapor with the stratosphere because the specific humidity of the rising air just below the tropopause is unrealistically low. The temperature increase in CAM3 occurs in a large region spanning the tropopause between 70 and 150 mb and between 30°S to 30°N. The increased temperatures are

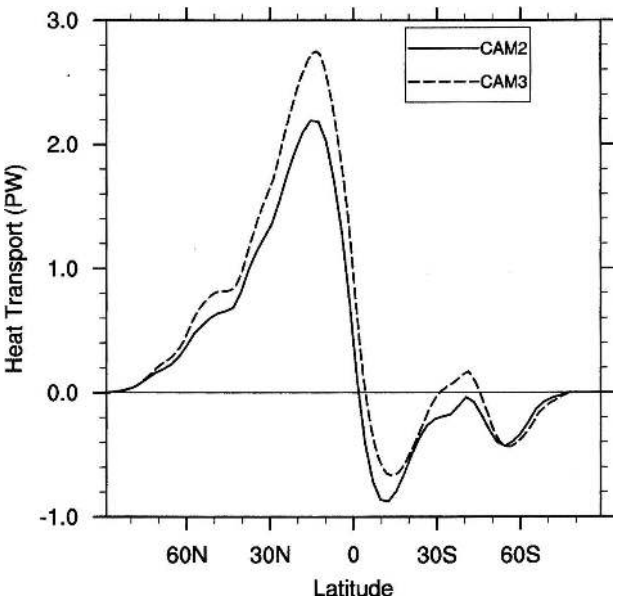

FIG. 6. Annual-mean implied meridional heat transport for CAM2 and CAM3.

in better agreement with the European Centre for Medium-Range Weather Forecasts (ECMWF) and National Centers for Environmental Prediction (NCEP) meteorological reanalysis (Kistler et al. 2001; Kållberg et al. 2004). The improvements are related to greater cirrus ice-water paths in CAM3 generated by the new cloud parameterizations (Boville et al. 2006). The maximum cold bias relative to both reanalyses is now between 4 and 5 K and occurs at approximately 70 mb on the equator (Fig. 7).

b. Spatial structure of tropical precipitation

Two aspects of the simulated precipitation have improved in CAM3 compared to CAM2. The double ITCZ in the Pacific is weaker in CAM3, and the precipitation is concentrated north of the equator as observed. In addition, the rainfall over some tropical continental areas has increased, particularly over several important rainforest regions.

The secondary peak in tropical precipitation south of the equator is much weaker than the northern peak in the annual and June–August (JJA) means in CAM3 (Fig. 8). The differences between the peak zonal-mean tropical precipitation in the Northern and Southern Hemispheres are shown in Table 2. It is evident from the table that CAM3 produces a more realistic interhemispheric gradient in tropical precipitation than CAM2 for these time periods. The improvement follows from a reduction in the evaporation efficiency for convective precipitation from CAM2 to CAM3. The mechanism for evaporation of precipitation (Sundqvist 1988) was introduced in CAM2 because of moisture biases that arose with updates to the longwave scheme (Collins et al. 2002a). Additional modifications to the longwave scheme for CAM3 have alleviated the moisture biases and permitted a reduction in the evaporation efficiency. However, CAM3 and CAM2 both produce stronger precipitation in the northern branch of the ITCZ during December–February (DJF), contrary to observations.

While CAM3 and CCSM3 still underestimate the precipitation for some midlatitude regions (Collins et al. 2006a), the rainfall over the greater Amazonian ba-

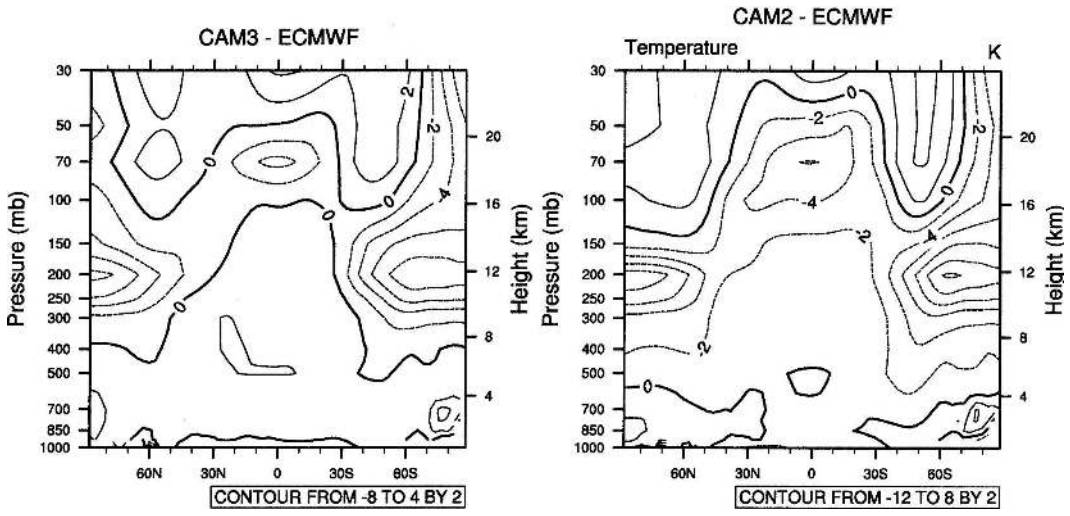

FIG. 7. Vertical profiles of the differences in atmospheric temperature (K, annually and zonally averaged): (left) CAM3 − ECMWF reanalysis and (right) CAM2 − ECMWF reanalysis. Dashed contours denote an underestimation of the temperature.

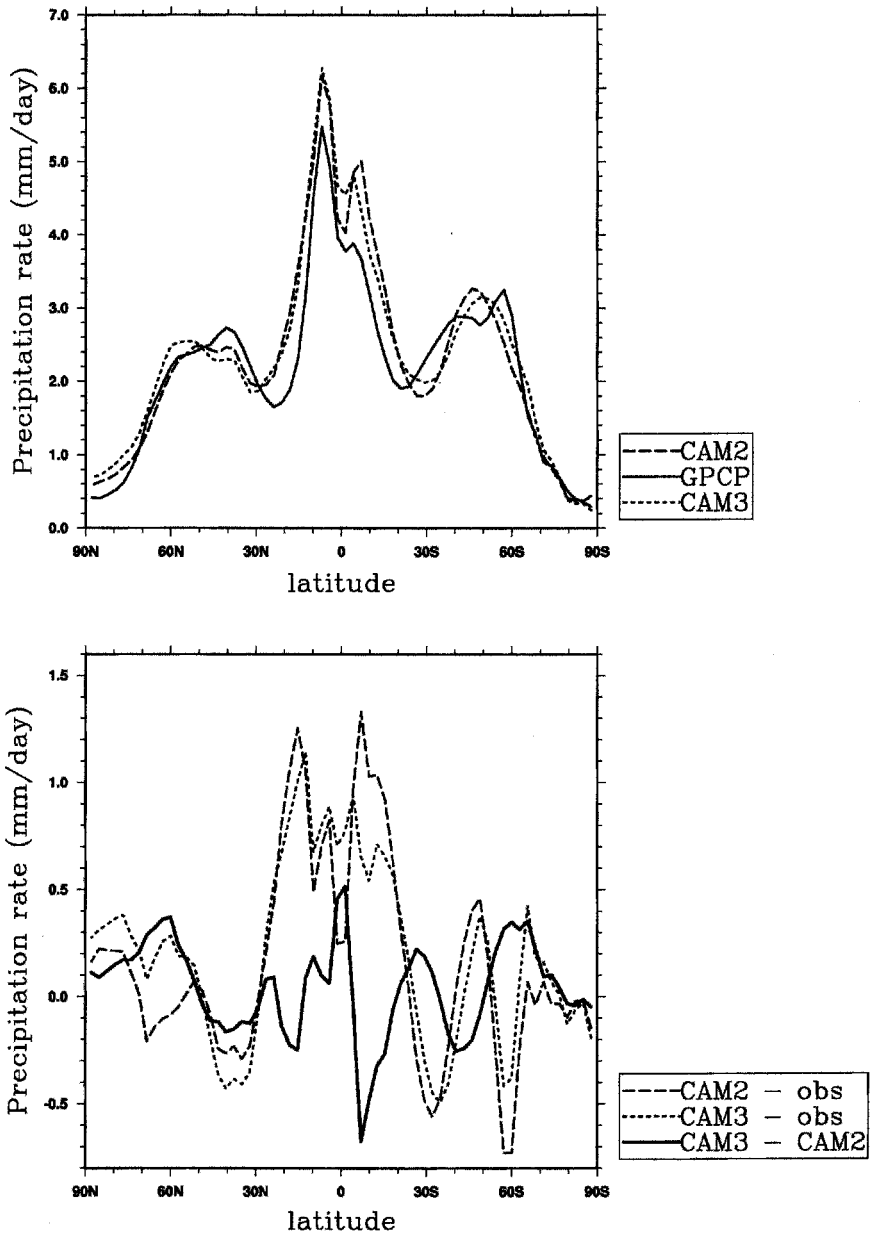

FIG. 8. Total precipitation (annually and zonally averaged) from (top) CAM2, CAM3, and GPCP, and (bottom) differences among the models and GPCP (obs) estimates.

sin (10°–0°S, 80°–50°W) is now closer to observational estimates. The annual rainfall is 92% of Global Precipitation Climatology Project (GPCP) estimates in CAM3, but only 78% of GPCP in CAM2. Similarly, during the rainiest season (JJA), the CAM3 rainfall is 74% of GPCP but the CAM2 rainfall is only 55% of GPCP. The improved fidelity of the tropical continental precipitation is important for simulations including dynamic vegetation (Levis et al. 2004; Bonan and Levis 2006) and the terrestrial carbon cycle. These improvements are caused by the reintroduction of convective

TABLE 2. Difference in zonal-mean precipitation maximums* (mm day^{-1}).

Period	CAM2	CAM3	GPCP**
Annual	1.1	1.6	1.6
DJF	1.1	0.9	−0.7
JJA	1.7	3.2	4.2

* The difference is the maximum zonal-mean precipitation between 0° and 10°N minus the maximum zonal-mean precipitation between 10°S and 0°.

** Adler et al. (2003).

TABLE 3. Indonesian cloud forcing statistics (10°S–20°N, 110°–160°E).

	CAM2		CAM3		ERBE[a]	
Period	s^b	ρ^c	s	ρ	s	ρ
Annual	−0.84	−0.65	−1.24	−0.81	−1.10	−0.94
DJF	−0.49	−0.61	−1.06	−0.89	−1.05	−0.93
JJA	−0.79	−0.74	−0.98	−0.82	−1.00	−0.96

[a] (Harrison et al. 1990; Kiehl and Trenberth 1997).
[b] Here, s is the linear least squares slope for SWCF as a function of LWCF.
[c] Here, ρ is the Pearson correlation coefficient between shortwave and longwave cloud forcing (SWCF and LWCF, respectively).

cloud fraction (section 2b) and by changes to the land surface model. The incorporation of convective cloud fraction helps improve the diurnal cycle of warm season convection over land. The changes to the land surface model help improve the surface temperatures and turbulent heat fluxes over sparsely vegetated continental regions (Dickinson et al. 2006).

c. Radiative effects of tropical clouds

The cloud systems in the Tropics are generally extensive, optically thick, and vertically distributed from the surface to the upper troposphere. As a result, these systems can reflect a significant fraction of incident sunlight and absorb a large fraction of the terrestrial radiation. Despite the large magnitudes of the shortwave and longwave cloud radiative effects, the net radiative effect of these systems on the top-of-atmosphere energy budget is near zero (Ramanathan et al. 1989; Cess et al. 2001). The cancellation implies that the shortwave and longwave cloud radiative effects should be linearly correlated with a slope close to −1, and this behavior is frequently observed in satellite observations. The statistics for the cloud radiative forcing for the Indonesian region (10°S–20°N, 110°–160°E) from CAM2, CAM3, and ERBE are given in Table 3.

Compared to ERBE, CAM2 underestimates the correlation of shortwave and longwave cloud radiative effects in all seasons examined. It also significantly underestimates the range of shortwave cloud radiative forcing. The statistics for CAM3 are in better agreement with the ERBE observations. The correlations of shortwave and longwave cloud forcing increase in all seasons, and the range of shortwave cloud forcing is now slightly overestimated in CAM3. The response of the shortwave cloud forcing to the warming of the mid Pacific during recent El Niño–Southern Oscillations (ENSOs) is also much more realistic in CAM3 (not shown). The improvement in the statistical cancellation of cloud forcing is due to three changes in the parameterizations for cloud processes. These are the reintroduction of convective cloud cover, the addition of sedimentation and advection of cloud condensate that increase the cloud water paths in midlevel convection, and the export of liquid water produced by the shallow convection scheme to the parameterizations of cloud condensate.

d. The 200-mb height field

The improvements in CAM3 can be quantified using a skill score for climate models based upon the fidelity of the climatological average 200-mb height field (Williamson 1995). The same score was applied to CCM3 and its preceding versions (Kiehl et al. 1998). It is a function of the height z_m produced by the model and the height z_a from a meteorological analysis. A perfect score of 0 indicates that the model is able to reproduce the exact 200-mb height field in the analysis. Let s_m and s_a represent the spatial variances of the modeled and analyzed height fields. Let an overbar denote an area average over the domain of interest. Then the score is given by the normalized mean square error (NMSE):

$$\mathrm{NMSE}(z_m) = \overline{(z_m - z_a)^2}/\overline{(z_a - \overline{z_a})^2}. \quad (1)$$

A scaled variance ratio (SVR) is included as a control statistic:

$$\mathrm{SVR}(z_m) = \left(\frac{s_m}{s_a}\right)^2 \mathrm{NMSE}(z_m). \quad (2)$$

The NMSE can be rewritten as a sum of three nonnegative terms:

$$\mathrm{NMSE}(z_m) = U(z_m) + C(z_m) + P(z_m). \quad (3)$$

The first term $U(z_m)$ is a measure of the unconditional bias in the model, and it vanishes only if the average heights in the model and analysis are equal. The second term $C(z_m)$ is a measure of the conditional bias in the model. It vanishes if linear regressions of the analyzed heights against the modeled heights yield slopes equal to unity. The third term $P(z_m)$ is a measure of phase errors, and it vanishes if the model and analysis fields are perfectly linearly correlated.

These scores have been computed for the 200-mb height field during January in the Northern Hemisphere. The results are displayed in Fig. 9 for each version of CCM and CAM. The results show that the NMSE and unconditional error $U(z_m)$ have declined with each successive version of CCM and CAM. The scores for CAM3 at T85 truncation are the lowest of any of the models. However, this version has slightly higher conditional and phase errors than CCM3. This

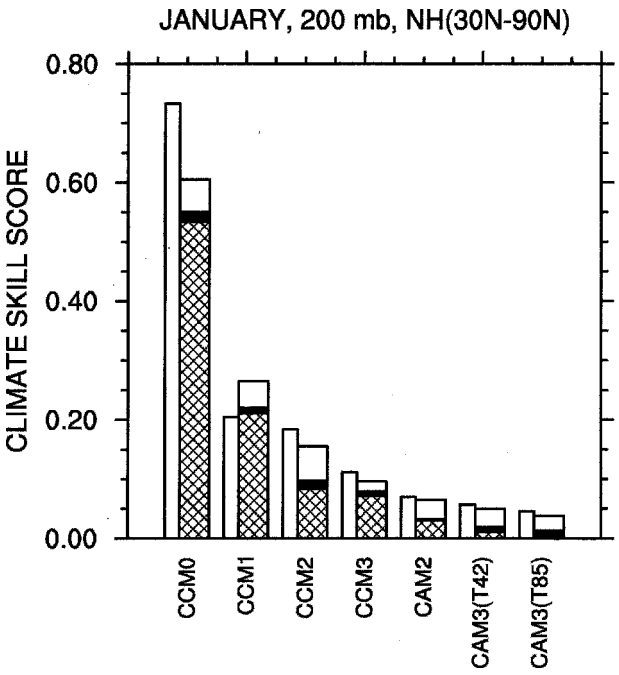

FIG. 9. NMSE and SVR for the 200-mb height field for each version of CCM and CAM. For each model version, the narrow left-hand-side bar is SVR(z_m) and the broad right-hand-side bar is NMSE(z_m). The terms in Eq. (3) for NMSE(z_m) are $U(z_m)$ (hatched), $C(z_m)$ (solid black), and $P(z_m)$ (unfilled).

graph illustrates the steady improvement in the upper tropospheric simulation in the CCM/CAM series.

5. Challenges for future development

Despite the improvements in the climate simulation produced by CAM3, there are still many significant challenges for future development. Issues with the implied heat transport, particularly in the Southern Hemisphere, are discussed in section 3. Several of the model deficiencies are discussed in the context of the CCSM3 integrations in Collins et al. (2006a), including:

- biases in midlatitude continental precipitation and surface temperature,
- errors in the radiative fluxes and surface stress in western coastal regions, and
- underestimation of downwelling shortwave radiation in polar regions.

For the sake of brevity, the following discussion clearly cannot be comprehensive, but it does serve to illustrate some problems in the climate simulations under investigation.

a. The Madden–Julian oscillation

Like its previous versions, CAM3 underestimates the variability associated with the Madden–Julian oscillation (MJO). This variability can be quantified from a time series of daily 200-mb zonal wind averaged over 10°S–10°N. The time series is bandpass filtered for a period of 20–100 days, and a MJO index is defined as the running 101-day variance of the bandpass-filtered data. The indices from the five-member ensemble are compared against the index from the NCEP reanalysis (Kistler et al. 2001) for the period 1981–2000. Table 4 compares the indices at the 50th, 90th, and 95th percentile from the ensemble and the reanalysis. The results show that while the model is able to reproduce the median variance with reasonable fidelity, it systematically underestimates the variance of the strongest fluctuations in zonal wind speed on these time scales. For the 90th and 95th percentiles, the model underestimates the variance by at least 25%. This systematic bias is also evident in Hovmöller diagrams of the bandpass-filtered 200-mb velocity potential in the Tropics.

The normalized power spectra for the 200-mb zonal velocity from the NCEP reanalysis and CAM3 are plotted in Fig. 10 for the tropical waveguide between 15°S and 15°N following the methodology of Wheeler and Kiladis (1999). In their analysis of tropical waves, Wheeler and Kiladis (1999) associate the MJO with eastward-propagating modes with periods between 30 and 96 days. It is evident from the figure that CAM3 systematically underestimates the power in eastward-traveling waves for periods between 30 and 60 days. However, the phase speeds of the waves in CAM3 in this frequency range are roughly consistent with the speeds of the corresponding waves in the reanalysis. For periods between 60 and 96 days, CAM3 generates too much (too little) power in westward-propagating (eastward propagating) modes. These results are consistent with the conclusions from the analysis of the MJO indices and show that CAM3 does not produce realistic MJO activity.

b. Energy budget of the western Pacific warm pool

The ability of the atmospheric model to produce a reasonable energy budget for the tropical western Pacific warm pool has important implications for the coupled simulation of the Pacific basin (Kiehl 1998;

TABLE 4. MJO indices* for 1981–2000 ($m^2 s^{-2}$).

Percentile	Min ensemble	Max ensemble	NCEP reanalysis
50	1.57	1.72	1.66
90	3.12	3.60	4.82
95	3.73	4.57	6.29

* The index is defined in section 5a.

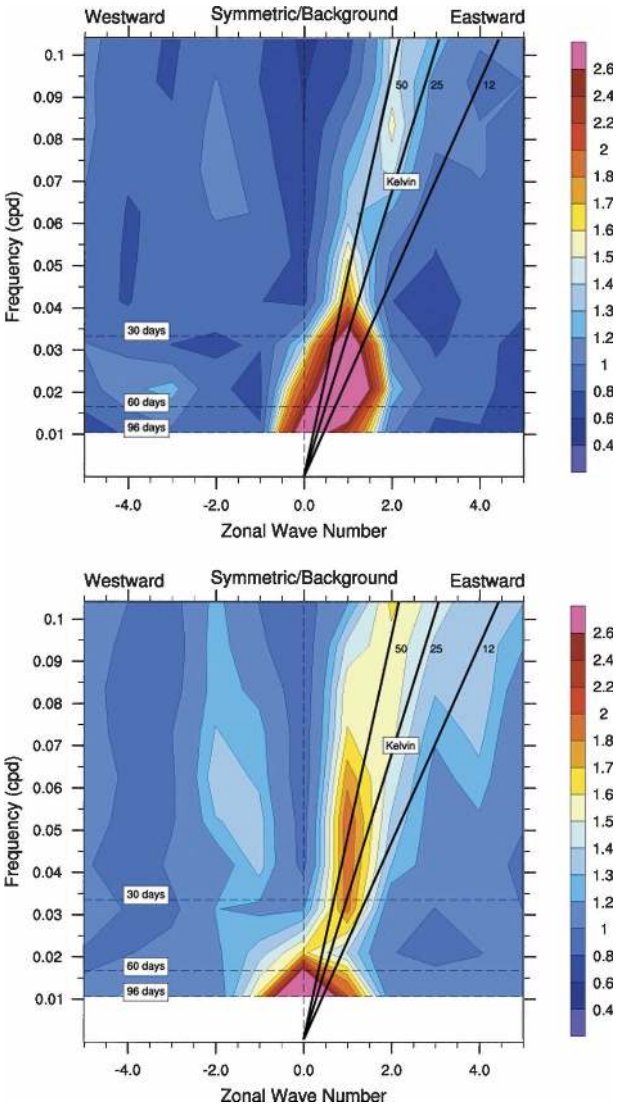

FIG. 10. Normalized power spectra for the 200-mb velocity fields summed over 15°S to 15°N for the (top) NCEP reanalysis and (bottom) CAM3. The spectra are normalized by smoothed background power spectra following Wheeler and Kiladis (1999). The solid lines are dispersion curves for odd meridional mode-numbered equatorial Kelvin waves for three equivalent depths of 12, 25, and 50 m.

Collins 2001a). Previous versions of CAM and CCM significantly overestimate the annual mean surface insolation over the warm pool. When the atmosphere is coupled to CCSM, this bias is compensated by latent heat fluxes much larger than the in situ estimates. The reason is that the ocean dynamical transport out of the warm pool is limited to less than approximately 20 W m^{-2}, so large net radiation inputs to the ocean must be balanced by other fluxes. The TOA and surface energy budgets for CAM2 and CAM3 are compared against observations in Table 5. The table shows that the estimate of the net surface energy budget in CAM3 is only 6 W m^{-2} greater than observed, while the net budget from CAM2 is 21 W m^{-2} greater than observed. The lower CAM3 energy budget is due to a 29 W m^{-2} reduction in surface insolation, which is partially compensated by decreases in the other fluxes. While the surface insolation in CAM3 is in better agreement with observations (e.g., Waliser et al. 1996), 22 W m^{-2} of the reduction is attributable to an overestimate of the TOA shortwave cloud radiative effect compared to ERBE. The remaining 7 W m^{-2} of the reduction is caused by the increased absorption of near-infrared radiation by water vapor in CAM3 (Collins et al. 2006b). The fact that the model is unable to match the TOA and surface all-sky shortwave fluxes simultaneously remains a basic research issue for future study. It should be noted that zonal-mean TOA cloud radiative effects are also overestimated for the entire Tropics, particularly the northern branch of the Hadley cell.

c. *Surface stress in the storm tracks*

CAM3 simulates larger surface stresses than observed in the storm tracks in both hemispheres. Since the biases appear throughout the annual cycle, it is sufficient to consider a comparison of the annual mean stress from CAM3 and the European Remote Sensing Satellite (ERS) scatterometer (Stoffelen and Anderson 1997a,b). The excess stress occurs in the southern Indian and Atlantic oceans adjacent to the Antarctic circumpolar current, the northern Atlantic between Nova Scotia and Great Britain, and the northern Pacific and Sea of Okhotsk (Fig. 11). In terms of zonal means, the peak errors at 52°N in the Northern Hemisphere and at 49°S in the Southern Hemisphere. At both latitudes, the stress is too large by 0.07 N m^{-2}. In the Northern Hemisphere, this constitutes an overestimate by 144%, while in the Southern Hemisphere the overestimate is by 56%. When the atmosphere is coupled to a dynamic ocean, these stress errors lead to ocean mass transports larger than observed, particularly in the Drake Passage (Large and Danabasoglu 2006). One possible explanation is that the total mountain stress is underestimated by the McFarlane (1987) scheme for gravity wave drag (GWD). The zonally averaged surface stress must match the eddy momentum flux convergence in the atmosphere. If the total surface stress over land, including the effects of vegetation and GWD, is too low, then the stress over ocean must be overestimated in order to match the atmospheric momentum flux convergence.

6. Summary

A new version of the Community Atmosphere Model, CAM3, has been developed and released to the

TABLE 5. Pacific warm pool energy budgets (10°S–10°N, 140°–170°E; W m^{-2}).

Level	Flux	CAM2	CAM3	Observation*
TOA	All-sky absorbed solar radiation	316	294	309
	Clear-sky absorbed solar radiation	373	381	373
	All-sky outgoing longwave radiation	227	212	225
	Clear-sky outgoing longwave radiation	279	282	285
Surface	All-sky absorbed solar radiation	227	198	182
	Clear-sky absorbed solar radiation	287	288	282
	All-sky upward longwave radiation	50	48	49
	Latent heat flux	125	118	107
	Sensible heat flux	13	9	8
	Net**	39	24	18

* References are given in Collins (2001a).

** The Net is the difference between the all-sky absorbed solar radiation and the sum of the latent heat flux, sensible heat flux, and all-sky longwave radiation.

scientific community. CAM3 includes new optional dynamical formulations and extensive improvements to the physical parameterizations. The model produces atmospheric simulations suitable for use in a fully coupled system that includes the land surface, full-depth ocean, and dynamic sea ice. The model physics is designed to maintain the fidelity of the simulations over a wide range of spatial resolutions and multiple dynamics. This is accomplished by making the model time step and other adjustable parameters dependent on the resolution and dynamics. The adjustable parameters affect the parameterizations of cloud and precipitation processes. The version of the model documented here is based upon the Eulerian spectral dynamics with T85 spectral truncation.

The new atmospheric model includes significant changes to cloud and precipitation processes, radiation processes, and treatments of aerosols. The finite volume dynamical core is now included as an option for integrating CAM. The tendency equations can be integrated with either process-split or time-split formulations of the numerical difference approximations. The physics of cloud and precipitation processes have been modified extensively. The modifications include separate treatments of liquid and ice condensate; advection, detrainment, and sedimentation of cloud condensate; and separate treatments of frozen and liquid precipitation. The radiation has been updated with a generalized treatment of cloud geometrical overlap and new treatment of longwave and shortwave interactions with water vapor. A prognostic sulfur cycle for predicting sulfate aerosols is now a standard option for the model. A prescribed distribution of sulfate, soil dust, carbonaceous species, and sea salt based upon a three-dimensional assimilation is used to calculate the direct effects of tropospheric aerosols on the heating rates. The model also includes the effects of stratospheric volcanic aerosols.

Several important features of the atmospheric simulation are improved in CAM3. The cold temperature bias at the tropical tropopause has been reduced by 60% relative to the ECMWF reanalysis. The overestimation of boreal winter sub-Arctic land surface temperatures has been reduced by 2 to 4 K in Eurasia, the western United States and Canada, and Greenland (Collins et al. 2006a). The surface precipitation over northern South America has increased from CAM2 to CAM3, although the model still does not produce enough rainfall over the Amazonian basin. The clear-sky longwave fluxes in polar regions are in much better agreement with observations. The structure of the ITCZ in the tropical Pacific is more realistic, with a weaker and less zonal SPCZ and stronger rainfall in the northern portion of the tropical Pacific warm pool. The relationship of shortwave and longwave effects for tropical cloud systems is more consistent with satellite observations. As a result, the response of cloud radiative forcing to ENSO variations has the correct sign and spatial structure in CAM3. The seasonal cycle of shortwave cloud forcing and cloud amount is more realistic in the northern Pacific and the coastal stratus regions.

A number of significant challenges remain for future study and development. Like the preceding models, CAM3 does not produce a reasonable simulation of the Madden–Julian oscillation. The amplitude of the 30–90-day variability is too low, and the wave trains do not consistently propagate eastward. The surface stress is much too large relative to satellite retrievals in the storm tracks, especially in the region just north of the Antarctic circumpolar current. As a result, the coupled model overestimates the mass transport through the Drake Passage by over 50%. However, the surface

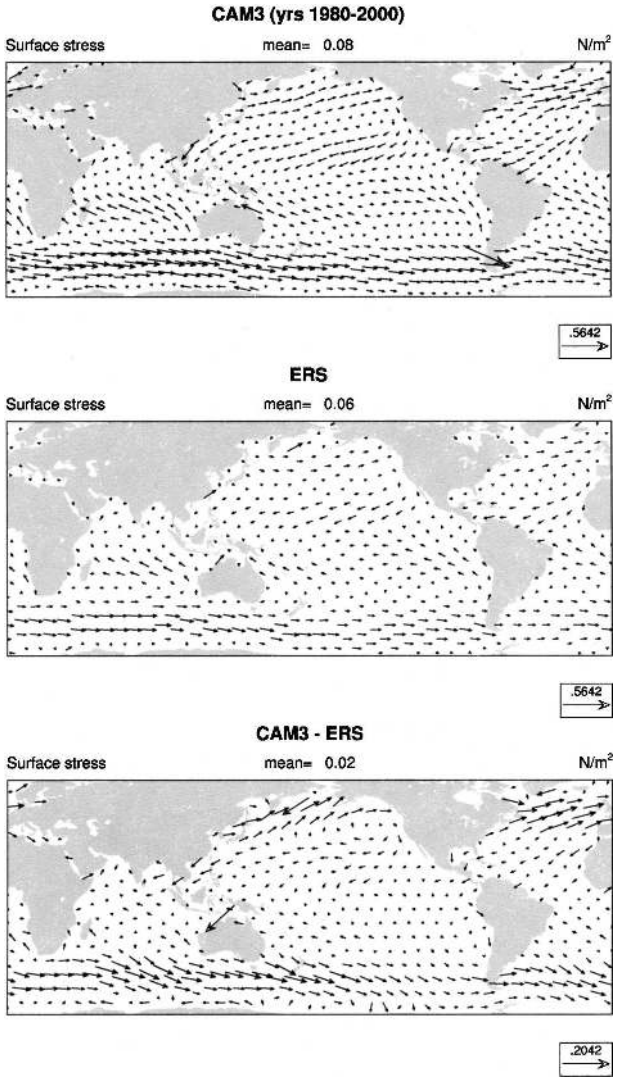

FIG. 11. (top) Annual-mean surface stress from CAM3, (middle) the ERS scatterometer, and (bottom) the difference between CAM3 and ERS. The orientation of the vectors corresponds to the wind direction, and the length of the vectors gives the magnitude of the surface wind stress.

stresses are still weaker than observed in the coastal stratus regions west of South America and Africa. There are biases of up to 100 m in the 500-mb height field, and the strength of the Aleutian low is too low and the strength of the Icelandic low is too high by roughly 6 mb (Hurrell et al. 2006).

Future development will focus on these and other systematic errors in the atmospheric simulation. The model is also being extended to include reactive chemistry and photochemistry from the troposphere through the thermosphere. Much more detailed treatments of the formation and evolution of the major aerosol species have also been brought online. The introduction of chemistry into CAM has elevated the importance of tracer transport and flux-form dynamics. Further progress in simulation fidelity will be measured in terms of both the physical and chemical state of the atmosphere.

Acknowledgments. The authors wish to acknowledge members of NCAR's Climate Modeling Section, Computer Software and Engineering Group, and Scientific Computing Division for their contributions to the development of CAM3. The suggestions by two anonymous reviewers have helped considerably to improve this description of CAM3.

The new model would not exist without the significant input from members of the CCSM Atmospheric Model Working Group too numerous to mention. Bill Collins (NCAR), Leo Donner (GFDL), James Hack (NCAR), David Randall (Colorado State University), and Phil Rasch (NCAR) were the co-chairs of the AMWG during the development of CAM3.

We would like to acknowledge the substantial contributions to the effort to develop CAM3 from the National Science Foundation, the Department of Energy, the National Aeronautics and Space Administration, and the National Oceanic and Atmospheric Administration.

This study is based on model integrations performed by NCAR and CRIEPI with support and facilities provided by NSF, DOE, MEXT, and ESC/JAMSTEC. We appreciate the financial support from the National Science Foundation for this special issue of the *Journal of Climate* on CCSM3.

REFERENCES

Adler, R. F., and Coauthors, 2003: The version-2 Global Precipitation Climatology Project (GPCP) monthly precipitation analysis (1979–present). *J. Hydrometeor.,* **4,** 1147–1167.

Ammann, C. M., G. A. Meehl, W. M. Washington, and C. S. Zender, 2003: A monthly and latitudinally varying volcanic forcing dataset in simulations of 20th century climate. *Geophys. Res. Lett.,* **30,** 1657, doi:10.1029/2003GL016875.

Barth, M. C., P. J. Rasch, J. T. Kiehl, C. M. Benkovitz, and S. E. Schwartz, 2000: Sulfur chemistry in the National Center for Atmospheric Research Community Climate Model: Description, evaluation, features and sensitivity to aqueous chemistry. *J. Geophys. Res.,* **105,** 1387–1415.

Bonan, G. B., and S. Levis, 2006: Evaluating aspects of the Community Land and Atmosphere Models (CLM3 and CAM3) using the CLM's dynamic global vegetation model. *J. Climate,* **19,** 2290–2301.

——, K. W. Oleson, M. Vertenstein, S. Levis, X. Zeng, Y. Dai, R. E. Dickinson, and Z.-L. Yang, 2002: The land surface climatology of the Community Land Model coupled to the NCAR Community Climate Model. *J. Climate,* **15,** 3123–3149.

Boville, B. A., and P. R. Gent, 1998: The NCAR Climate System Model, version 1. *J. Climate,* **11,** 1115–1130.

——, and C. S. Bretherton, 2003: Heating and dissipation in the NCAR Community Atmosphere Model. *J. Climate,* **16,** 3877–3887.

——, P. J. Rasch, J. J. Hack, and J. R. McCaa, 2006: Representation of clouds and precipitation processes in the Community Atmosphere Model version 3 (CAM3). *J. Climate,* **19,** 2184–2198.

Briegleb, B. P., C. M. Bitz, E. C. Hunke, W. H. Lipscomb, M. M. Holland, J. L. Schramm, and R. E. Moritz, 2004: Scientific description of the sea ice component in the Community Climate System Model, Version Three. Tech. Rep. NCAR/TN-463+STR, National Center for Atmospheric Research, Boulder, CO, 78 pp.

Cess, R. D., M. Zhang, B. A. Wielicki, D. F. Young, X.-L. Zhou, and Y. Nikitenko, 2001: The influence of the 1998 El Niño upon cloud–radiative forcing over the Pacific warm pool. *J. Climate,* **14,** 2129–2137.

Clough, S. A., F. X. Kneizys, and R. W. Davies, 1989: Line shape and the water vapor continuum. *Atmos. Res.,* **23,** 229–241.

Collins, W. D., 2001a: Effects of enhanced shortwave absorption on coupled simulations of the tropical climate system. *J. Climate,* **14,** 1147–1165.

——, 2001b: Parameterization of generalized cloud overlap for radiative calculations in general circulation models. *J. Atmos. Sci.,* **58,** 3224–3242.

——, P. J. Rasch, B. E. Eaton, B. Khattatov, J.-F. Lamarque, and C. S. Zender, 2001: Simulating aerosols using a chemical transport model with assimilation of satellite aerosol retrievals: Methodology for INDOEX. *J. Geophys. Res.,* **106,** 7313–7336.

——, J. K. Hackney, and D. P. Edwards, 2002a: A new parameterization for infrared emission and absorption by water vapor in the National Center for Atmospheric Research Community Atmosphere Model. *J. Geophys. Res.,* **107,** 8028, doi:10.1029/2000JD000032.

——, P. J. Rasch, B. A. Eaton, D. W. Fillmore, J. T. Kiehl, T. C. Beck, and C. S. Zender, 2002b: Simulation of aerosol distributions and radiative forcing for INDOEX: Regional climate impacts. *J. Geophys. Res.,* **107,** 4664, doi:10.1029/2001JD001365.

——, and Coauthors, 2004: Description of the NCAR Community Atmosphere Model (CAM3). Tech. Rep. NCAR/TN-464+STR, National Center for Atmospheric Research, Boulder, CO, 226 pp.

——, and Coauthors, 2006a: The Community Climate System Model version 3 (CCSM3). *J. Climate,* **19,** 2122–2143.

——, J. M. Lee-Taylor, D. P. Edwards, and G. L. Francis, 2006b: Effects of increased near-infrared absorption by water vapor on the climate system. *J. Geophys. Res.,* in press.

Dickinson, R. E., K. W. Oleson, G. Bonan, F. Hoffman, P. Thornton, M. Vertenstein, Z.-L. Yang, and X. Zeng, 2006: The Community Land Model and its climate statistics as a component of the Community Climate System Model. *J. Climate,* **19,** 2302–2324.

EROS Data Center, 2004: GTOPO30 documentation. [Available online at http://lpdaac.usgs.gov/gtopo30/README.asp.]

Hack, J. J., B. A. Boville, B. P. Briegleb, J. T. Kiehl, P. J. Rasch, and D. L. Williamson, 1993: Description of the NCAR Community Climate Model (CCM2). Tech. Rep. NCAR/TN-382+STR, National Center for Atmospheric Research, 120 pp.

——, J. M. Caron, S. G. Yeager, K. W. Oleson, M. M. Holland, J. E. Truesdale, and P. J. Rasch, 2006: Simulation of the global hydrological cycle in the CCSM Community Atmosphere Model version 3 (CAM3): Mean features. *J. Climate,* **19,** 2199–2221.

Harrison, E. F., P. Minnis, B. R. Barkstrom, V. Ramanathan, R. D. Cess, and G. G. Gibson, 1990: Seasonal variation of cloud radiative forcing derived from the Earth Radiation Budget Experiment. *J. Geophys. Res.,* **95,** 18 687–18 703.

Hurrell, J. W., J. J. Hack, A. Phillips, J. Caron, and J. Yin, 2006: The dynamical simulation of the Community Atmospheric Model Version 3 (CAM3). *J. Climate,* **19,** 2162–2183.

Kållberg, P., A. Simmons, S. Uppala, and M. Fuentes, 2004: The ERA-40 archive. Tech. Rep. ERA-40 Project Rep. 17, European Centre for Medium-Range Weather Forecasts, Reading, United Kingdom, 35 pp.

Kiehl, J. T., 1998: Simulation of the tropical Pacific warm pool with the NCAR Climate System Model. *J. Climate,* **11,** 1342–1355.

——, and K. E. Trenberth, 1997: Earth's annual global mean energy budget. *Bull. Amer. Meteor. Soc.,* **78,** 197–208.

——, and P. R. Gent, 2004: The Community Climate System Model, Version Two. *J. Climate,* **17,** 3666–3682.

——, J. Hack, G. Bonan, B. Boville, B. Briegleb, D. Williamson, and P. Rasch, 1996: Description of the NCAR Community Climate Model (CCM3). Tech. Rep. NCAR/TN-420+STR, National Center for Atmospheric Research, Boulder, CO, 152 pp.

——, J. J. Hack, G. B. Bonan, B. B. Boville, D. L. Williamson, and P. J. Rasch, 1998: The National Center for Atmospheric Research Community Climate Model: CCM3. *J. Climate,* **11,** 1131–1149.

King, M. D., and Coauthors, 2003: Cloud and aerosol properties, precipitable water, and profiles of temperature and water vapor from MODIS. *IEEE Trans. Geosci. Remote Sens.,* **41,** 442–458.

Kistler, R., and Coauthors, 2001: The NCEP–NCAR 50-year reanalysis: Monthly means CD-ROM and documentation. *Bull. Amer. Meteor. Soc.,* **82,** 247–267.

Klein, S. A., and D. L. Hartmann, 1993: The seasonal cycle of low stratiform clouds. *J. Climate,* **6,** 1587–1606.

Large, W. G., and G. Danabasoglu, 2006: Attribution and impacts of upper ocean biases in CCSM3. *J. Climate,* **19,** 2325–2346.

Levis, S., G. B. Bonan, M. Vertenstein, and K. W. Oleson, 2004: The Community Land Model's Dynamic Global Vegetation Model (CLM-DGVM): Technical description and user's guide. Tech. Rep. NCAR/TN-459+IA, National Center for Atmospheric Research, Boulder, CO, 50 pp.

Levitus, S., 1982: *Climatological Atlas of the World Ocean.* NOAA Professional Paper 13, National Oceanic and Atmospheric Administration, 173 pp.

Lin, S.-J., 2004: A vertically Lagrangian finite-volume dynamical core for global models. *Mon. Wea. Rev.,* **132,** 2293–2307.

——, and R. B. Rood, 1996: Multidimensional flux-form semi-Lagrangian transport schemes. *Mon. Wea. Rev.,* **124,** 2046–2070.

Locatelli, J., and P. Hobbs, 1974: Fall speeds and masses of solid precipitation particles. *J. Geophys. Res.,* **79,** 2185–2197.

McFarlane, N. A., 1987: The effects of orographically excited gravity wave drag on the general circulation of the lower stratosphere and troposphere. *J. Atmos. Sci.,* **44,** 1775–1800.

Oleson, K. W., and Coauthors, 2004: Technical description of the Community Land Model (CLM). Tech. Rep. NCAR/TN-461+STR, National Center for Atmospheric Research, Boulder, CO, 174 pp.

Ramanathan, V., R. D. Cess, E. F. Harrison, P. Minnis, B. R. Barkstrom, E. Ahmad, and D. Hartmann, 1989: Cloud-radiative forcing and climate: Results from the Earth Radiation Budget Experiment. *Science,* **243,** 57–63.

Randel, D. L., T. H. Vonder Haar, M. A. Ringerud, G. Stephens, T. J. Greenwald, and C. L. Combs, 1996: A new global water vapor dataset. *Bull. Amer. Meteor. Soc.,* **77,** 1233–1246.

Rasch, P. J., and J. E. Kristjánsson, 1998: A comparison of the CCM3 model climate using diagnosed and predicted condensate parameterizations. *J. Climate,* **11,** 1587–1614.

——, M. C. Barth, J. T. Kiehl, S. E. Schwartz, and C. M. Benkovitz, 2000: A description of the global sulfur cycle and its controlling processes in the National Center for Atmospheric Research Community Climate Model, Version 3. *J. Geophys. Res.,* **105,** 1367–1385.

——, W. D. Collins, and B. E. Eaton, 2001: Understanding the Indian Ocean Experiment (INDOEX) aerosol distributions with an aerosol assimilation. *J. Geophys. Res.,* **106,** 7337–7356.

——, D. B. Coleman, N. Mahowald, D. L. Williamson, S.-J. Lin, B. A. Boville, and P. Hess, 2006a: Characteristics of atmospheric transport using three numerical formulations for atmospheric dynamics in a single GCM framework. *J. Climate,* **19,** 2243–2266.

——, and Coauthors, 2006b: Characterization of tropical transient activity in the CAM3 atmospheric hydrologic cycle. *J. Climate,* **19,** 2222–2242.

Rayner, N. A., D. E. Parker, E. B. Horton, C. K. Folland, L. V. Alexander, D. P. Powell, E. C. Kent, and A. Kaplan, 2003: Global analyses of sea surface temperature, sea ice, and night marine air temperature since the late nineteenth century. *J. Geophys. Res.,* **108,** 4407, doi:10.1029/2002JD002670.

Reynolds, R., N. Rayner, T. Smith, D. Stokes, and W. Wang, 2002: An improved in situ and satellite SST analysis for climate. *J. Climate,* **15,** 1609–1625.

Rossow, W. B., and R. A. Schiffer, 1999: Advances in understanding clouds from ISCCP. *Bull. Amer. Meteor. Soc.,* **80,** 2261–2287.

Rothman, L. S., and Coauthors, 2003: The HITRAN molecular spectroscopic database: Edition of 2000 including updates of 2001. *J. Quant. Spectrosc. Radiat. Transfer,* **82,** 5–42.

Smith, R. D., and P. R. Gent, cited 2002: Reference manual for the Parallel Ocean Program (POP), ocean component of the Community Climate System Model (CCSM2.0 and 3.0). Tech. Rep. LA-UR-02-2484, Los Alamos National Laboratory. [Available online at http://www.ccsm.ucar.edu/models/ccsm3.0/pop.]

Stoffelen, A., and D. Anderson, 1997a: Scatterometer data interpretation: Estimation and validation of the transfer function CMOD4. *J. Geophys. Res.,* **102,** 5767–5780.

——, and ——, 1997b: Scatterometer data interpretation: Measurement space and inversion. *J. Atmos. Oceanic Technol.,* **14,** 1298–1313.

Sundqvist, H., 1988, Parameterization of condensation and associated clouds in models for weather prediction and general circulation simulation. *Physically-based Modelling and Simulation of Climate and Climate Change,* Vol. 1, M. E. Schlesinger, Ed., Kluwer Academic, 433–461.

Waliser, D. E., W. D. Collins, and S. P. Anderson, 1996: An estimate of the surface shortwave cloud forcing over the western Pacific during TOGA COARE. *Geophys. Res. Lett.,* **23,** 519–522.

Washington, W. M., 1982: Documentation for the Community Climate Model (CCM), Version Ø. Tech. Rep., National Center for Atmospheric Research, Boulder, CO, 222 pp.

Wheeler, M. C., and G. N. Kiladis, 1999: Convectively coupled equatorial waves: Analysis of clouds and temperature in the wavenumber-frequency domain. *J. Atmos. Sci.,* **56,** 374–399.

Williamson, D. L., 1983: Description of NCAR Community Climate Model (CCM0B). Tech. Rep. NCAR/TN-210+STR, National Center for Atmospheric Research, Boulder, CO, 88 pp.

——, 1995: Skill scores from the AMIP simulations. *Proc. First Int. AMIP Scientific Conf.,* Monterey, CA, World Meteorological Organization, 253–256.

——, 2002: Time-split versus process-split coupling of parameterizations and dynamical core. *Mon. Wea. Rev.,* **130,** 2024–2041.

——, J. T. Kiehl, V. Ramanathan, R. E. Dickinson, and J. J. Hack, 1987: Description of NCAR Community Climate Model (CCM1). Tech. Rep. NCAR/TN-285+STR, National Center for Atmospheric Research, Boulder, CO, 112 pp.

Xu, K.-M., and S. K. Krueger, 1991: Evaluation of cloudiness parameterizations using a cumulus ensemble model. *Mon. Wea. Rev.,* **119,** 342–367.

Zdunkowski, W. G., W.-G. Panhans, R. M. Welch, and G. J. Korb, 1982: A radiation scheme for circulation and climate models. *Contrib. Atmos. Phys.,* **55,** 215–238.

Zhang, M., W. Lin, C. B. Bretherton, J. J. Hack, and P. J. Rasch, 2003: A modified formulation of fractional stratiform condensation rate in the NCAR Community Atmosphere Model (CAM2). *J. Geophys. Res.,* **108,** 4035, doi:10.1029/2002JD002523.

Zhang, Y. C., W. B. Rossow, A. A. Lacis, V. Oinas, and M. I. Mishchenko, 2004: Calculation of radiative fluxes from the surface to top of atmosphere based on ISCCP and other global data sets: Refinements of the radiative transfer model and the input data. *J. Geophys. Res.,* **109,** D19105, doi:10.1029/2003JD004457.